

# Effects of natural zeolite and sulfate ions on the mechanical properties and microstructure of plastic concrete

Ali AKBARPOUR\*, Mahdi MAHDIKHANI, Reza Ziae MOAYED

Civil Engineering Department, Imam Khomeini International University, Qazvin 34149-16818, Iran

\*Corresponding author. E-mail: akbarpour.ali8@gmail.com

© Higher Education Press 2021

**ABSTRACT** One of the strategic materials used in earth-fill embankment dams and in modifying and preventing groundwater flow is plastic concrete (PIC). PIC is comprised of aggregates, water, cement, and bentonite. Natural zeolite (NZ) is a relatively abundant mineral resource and in this research, the microstructure, unconfined strength, triaxial behavior, and permeability of PIC made with 0%, 10%, 15%, 20%, and 25% replacement of cement by NZ were studied. Specimens of PIC-NZ were subjected to confined conditions and three different confining pressures of 200, 350, and 500 kPa were used to investigate their mechanical behavior and permeability. To study the effect of sulfate ions on the properties of PIC-NZ specimens, the specimens were cured in one of two different environments: normal condition and in the presence of sulfate ions. Results showed that increasing the zeolite content decreases the unconfined strength, elastic modulus, and peak strength of PIC-NZ specimens at the early ages of curing. However, at the later ages, increasing the zeolite content increases unconfined strength as well as the peak strength and elastic modulus. Specimens cured in the presence of sulfate ions indicated lower permeability, higher unconfined strength, elastic modulus, and peak strength due to having lower porosity.

**KEYWORDS** plastic concrete, sulfate resistance, natural zeolite, triaxial compression test, SEM, permeability

## 1 Introduction

Plastic concrete (PIC) is comprised of cement, water, aggregates, and bentonite. PIC offers an efficient way to control dam seepage [1–3]. In addition, utilizing bentonite in concrete is an effective method of eliminating heavy metals [4]. Compared with conventional concrete, PIC has excellent ductility after reaching failure, and it also has low hydraulic conductivity [5,6]. To avert the instability of diaphragm walls and to meet the deformation compatibility requirements of such walls with the surrounding soil, International Committee of Large Dams (ICOLD) recommends that the modulus of elasticity of a diaphragm wall should be 1 to 5 times higher than the elastic modulus of contiguous soil [7]. To attain low elastic modulus requirements, the water/cement ratio of PIC is

high—in the range of 1.5–4 [8,9]. PIC, due to its required usage, needs to have low permeability. Note that the permeability of such materials depends on the *w/c* ratio, and that it should be anticipated that the permeability of PIC is much higher than conventional concretes. Indeed, development of a method that will not only satisfy the low permeability requirements of PIC but also will not increase its elastic modulus needs considerable efforts [10].

One serious sustainability issue facing the concrete industries is that of carbon dioxide emitted from manufacturing ordinary Portland cement. Carbon dioxide emissions attract global attention because it is the major factor causing global warming. 7% of the global CO<sub>2</sub> emissions are an outcome of manufacturing Portland cement [11]. The calcination of limestone is the prime reason, responsible for the 60% of these emissions [12]. Regarding an average clinker factor of 0.78, cement manufacturing is responsible for 2.3 billion Mt of annual

worldwide CO<sub>2</sub> emissions [13]. The remaining CO<sub>2</sub> emissions come from fuel combustion, which is required for generating heat needed for the reactions forming clinker. In the last two decades, monumental achievements in energy efficiency have been made in Portland cement production even though the calcination of limestone has remained a significant source of CO<sub>2</sub> emissions [14]. It should be mentioned that the above numbers relate only to direct emissions; based on economic input-output analysis-based life-cycle assessments (EIO-LCA) using U.S. data [15], life-cycle greenhouse gas emissions associated with the manufacture of Portland cement are expected to be 13% higher than direct emission. Thus, the construction industry is in dire need of finding alternative materials to replace cement.

The usage of supplementary cementitious materials (SCMs) provides an effective way to pare down the amount of CO<sub>2</sub> emissions from limestone calcination. A study involving academics and business leaders [16] pointed out that new generation of construction materials is one of the seven most promising investment fields. It reported that low carbon cement poses “the biggest single opportunity for CO<sub>2</sub> reduction”. It concluded that if a low carbon alternative replaced 50% of Portland cement, it could lead to 1 billion Mt of CO<sub>2</sub> emission cut annually. On the other hand, in the U.S., more than 60% of ready-mixed concrete uses SCMs, which are usually added to concrete instead of being blended with clinker [5]. According to USGS data [17], 1.7 billion Mt of alternative materials are needed to replace 50% of Portland cement. The global availability of fly ash and ground-granulated-blast furnace slag is approximately 800 [18] and 300 million Mt [19], respectively, which is roughly half of the required amount of alternative materials. Thus, there is a strong need to explore other SCMs and their effect on concrete properties.

Natural zeolite is a mineral resource that exists abundantly. It is a volcanic or volcano-sediment material with a skeletal crystal structure. This has voids occupied by ions and molecules of water with significant freedom of movement that allows reversible hydration and ion exchange [20,21]. The utilization of natural zeolite in cement pastes reduces the number of harmful large pores ( $d > 938 \text{ \AA}$ ) and increases the number of micropores ( $d < 625 \text{ \AA}$ ), so an improvement in concrete strength and other properties can be expected. A decrease in calcium hydroxide content and an increase in the C-S-H phase stem from an increase in the mass ratio of SiO<sub>2</sub>/CaO in the transition zone by utilizing natural zeolite [22,23]. This improves the structure of the transition zone, which increases the strength and decreases the permeability of concrete [24–26].

Moreover, because of the most important application of

PIC, which is in earth dam cut-off walls, it is crucial to study its sulfate resistance. Chloride attack [27] and sulfate attack [28] could be detrimental actions. Groundwater and soil, marine environments, industrial processes, etc., are possible extraneous sources of sulfates, whilst concrete constituents such as aggregates, mixing water, cement, and natural pozzolans are potential sources of sulfates [29]. The resistance to sulfate attack is the main factor determining concrete durability [30,31]. The calcium sulfate dihydrate CaSO<sub>4</sub>·2H<sub>2</sub>O (marked as gypsum) and calcium sulfoaluminate 3CaO·Al<sub>2</sub>O<sub>3</sub>·3CaSO<sub>4</sub>·32H<sub>2</sub>O (marked as ettringite) are two primary products that derive from sulfate actions on cement-based materials [32]. Secondary effects contain the loss of cementitious structure and the decalcification of C-S-H gel. Decalcification is the phenomenon of continuous depletion of the C/S ratio within the C-S-H gel. Ettringite formed at early ages is referred to as “primary ettringite”. Ettringite formed by recrystallization and dissolution in cracks and void spaces is often referred to as “secondary ettringite” [33]. There is a need to understand the effects of zeolite as a SCM on the sulfate resistance of PIC.

In the present study, the effects of natural zeolite on sulfate resistance, mechanical properties, and permeability of plastic concrete were studied. Since plastic concrete's most important application is to be buried in soil, it will always be in danger of sulfate attack, so there is a need to study its sulfate resistance. The mechanical properties and permeability of plastic concrete containing natural zeolite were studied in this work, which included investigation of specimens that were cured in containers to simulate sulfate attack. In addition, since PIC is usually utilized for applications involving burial in the soil, its mechanical properties should be studied in confined conditions to simulate the effect of the surrounding soil. New apparatus and procedure of performing permeability test were designed and executed to record the coefficient of permeability of concrete specimens in confined conditions. In addition, in order to evaluate the effects of natural zeolite on the mechanical properties of PIC, triaxial and uniaxial compression tests were performed at four different ages. Moreover, in order to study the microstructure of PIC, SEM (Scanning Electron Microscopy) images and X-ray diffraction patterns were utilized.

## 2 Experimental procedure

### 2.1 Materials

In accordance with ASTM C150/C150M-11 [34], the cement used was type II Portland cement. Also, the

clinoptilolite type of natural zeolite was used in this study. **Table 1** represents the chemical and mineralogical composition of cement and natural zeolite. Coarse aggregates were classified into two different size groups, 9.5–19 mm and 4.75–9.5 mm. Coarse aggregates had a specific gravity of 1.7 and water absorption of 2.3%. A crushed type of fine aggregates with a specific gravity of 1.55 and water absorption of 3.4% was utilized in this study. The particle size distribution curve of sand and gravel incorporated in this study are illustrated in **Fig. 1**. In accordance with ICOLD recommendations [7], to ensure uniform distribution of bentonite particles that would lead to a homogenous mixture, bentonite powder and required amount of water were thoroughly mixed by a high-speed mixer 24 h before being combined with aggregates and cementitious materials, because bentonite materials have high water absorption and low permeability. **Table 2** represents the mechanical and physical properties of bentonite. The chemical

**Table 1** Chemical and mineralogical composition of cement and zeolite

compound/property	cement	natural zeolite
calcium oxide (CaO)	61.26%	4.2%
silica (SiO <sub>2</sub> )	20.53%	66.24%
alumina (Al <sub>2</sub> O <sub>3</sub> )	3.91%	12.79%
Iron oxide (Fe <sub>2</sub> O <sub>3</sub> )	3.72%	1.29%
Magnesium oxide (MgO)	3.65%	1.18%
Sodium oxide (Na <sub>2</sub> O)	0.41%	1.98%
Potassium oxide (K <sub>2</sub> O)	0.95%	1.39%
Sulfur trioxide (SO <sub>3</sub> )	2.97%	0.48%
Titanium Dioxide (TiO <sub>2</sub> )	0.27%	–
Loss on Ignition (L.O.I)	1.51%	10.31%
C <sub>2</sub> S	23.57%	–
C <sub>3</sub> S	51.33%	–
C <sub>3</sub> A	5.56%	–
C <sub>4</sub> AF	8.24%	–
specific gravity	3.12	2.18
specific surface	3060 cm <sup>2</sup> /g	10000 cm <sup>2</sup> /g

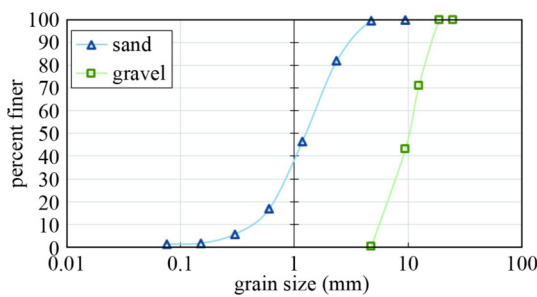


**Fig. 1** Particle size distribution curve of aggregates.

characteristics of bentonite are presented in **Table 3**. The cation exchange capacity of bentonite was measured according to ASTM D7503 [35]. In order to record the cation exchange capacities of bentonite various methods can be used. The most widely used methods involve the replacement of the interlayer cations with index cations in a known volume solution and then to do analytical determination of the cations in the solution by standard techniques. One important aspect critical in measuring the cation exchange capacities of bentonite is use of cations that are preferred to the cations being displaced. For instance, Cs<sup>+</sup>, Ba<sup>+</sup>, and NH<sub>4</sub><sup>+</sup> can be used as index cations.

## 2.2 Mixture proportioning

To explore the effects of natural zeolite replacement on the properties of PLC, cement was replaced with five different proportions of Natural zeolite (NZ): 0%, 10%, 15%, 20%, and 25% of total cementitious materials by weight. Some of the specimens are shown in **Fig. 2**. In all mixtures, the water/cementitious materials ratio and total cementitious materials were kept constant at 2.94 and 152.7 kg/m<sup>3</sup>, respectively. **Table 4** represents the mixture proportions.

## 2.3 Test methods

To evaluate the effect of sulfate ions on the microstructure and mechanical properties of PLC-NZ, all the specimens of the same mix design were fully immersed in two different containers until tested, one in the normal condition (lime water) and the other in a container simulating sulfate attack. Na<sub>2</sub>SO<sub>4</sub> (Na<sup>+</sup> cation) was utilized for preparing artificial sulfate solution for this purpose. The mass fraction of sulfate solution was 6%.

**Table 2** Mechanical and physical properties of bentonite

property	value
specific gravity	2.79
pH (1 : 10, soil-water ratio)	9.5
specific surface area, (m <sup>2</sup> /kg) × 10 <sup>-3</sup>	413

**Table 3** Chemical characteristics of bentonite

characteristics	content
CEC (cmol/kg, soil)	68.2
organic content (%)	1.4
carbonate content (%)	8
exchangeable K <sup>+</sup> (cmol/kg)	3.4
exchangeable Ca <sup>2+</sup> (cmol/kg)	14.2
exchangeable Na <sup>+</sup> (cmol/kg)	48.5
exchangeable Mg <sup>2+</sup> (cmol/kg)	2.1

Note: mineral composition in decreasing abundance: montmorillonite, calcite, quartz.

After that, the pH of the solution in the container simulating sulfate attack always remained at pH 3 by use of sulfuric acid.

### 2.3.1 Unconfined compression test

To evaluate the evolution of compressive strength and the contribution of NZ on the strength of PIC specimens, PIC-NZ cubes of 10 cm size were prepared. Specimens were tested at four different ages of 7, 14, 28, and 90 d; this was to assess the effect of curing time on strength gained, and also to illuminate the effects of sulfate ions on the strength of specimens by the passage of time. Regarding the low strength levels of PIC-NZ specimens, the rate of load application was decreased so that the failures of PIC-NZ specimens occur during  $70 \pm 10$  s after the start of loading [10].

### 2.3.2 Triaxial compression test

Triaxial compression tests were performed in three different confining pressures of 200, 350, and 500 kPa to model the effect of surrounding soil on the mechanical behavior of PIC-NZ specimens. PIC-NZ specimens were tested at four different ages of 7, 14, 28, and 90 d. The same type of loading path was followed in all tests. In this regard, a hydrostatic test inaugurated the triaxial compression test. Once the confining pressure reached its desired amount, it was kept constant, and the specimen started to be loaded axially. The axial rate equal to  $0.005 \text{ min}^{-1}$  was selected, based on the recommendations of



**Fig. 2** Cubic and cylindrical PIC-NZ specimens.

ASTM-D2850 [36] and ASTM-D2166 [37] for triaxial and unconfined test on cohesive soil. Regarding the cylindrical  $\phi 10 \text{ cm} \times 20 \text{ cm}$  specimens for the triaxial compression test, the corresponding speed of the piston for this rate of specimen loading was equal to  $0.1 \text{ mm/min}$  [38–40].

### 2.3.3 Permeability

For the application of PIC, permeability is a critical factor. To evaluate the permeability of PIC-NZ specimens while they are subjected to a confining pressure, new apparatus and procedure for performing permeability tests were designed and executed.  $\phi 10 \text{ cm} \times 6 \text{ cm}$  specimens were prepared for this test. Three different confining pressures of 200, 350, and 500 kPa were used. To eliminate sidewall leakage, both top and bottom caps were attached to the specimens using RTV silicone adhesive sealant. Two rubber membranes were placed around the specimens, and two O-rings of diameter 70 and 100 mm were used at each end to seal the PIC-NZ specimens. Specimens were tested at the ages of 28, 56, and 90 d.

---

## 3 Test results

### 3.1 Mechanical behavior of plastic concrete-natural zeolite

#### 3.1.1 Effect of zeolite content and specimen age

The uniaxial compression test was carried out on  $10 \text{ cm} \times 10 \text{ cm} \times 10 \text{ cm}$  specimens to explore the mechanical behavior of PIC-NZ specimens. Figure 3 represents the evolution with time of compressive strength of PIC mixes containing different proportions of natural zeolite. As can be seen, extending the curing time decreased the porosity, which increased the compressive strength of the specimens. In general, hydration reactions occur when cement is exposed to water. As the hydration proceeds, the particles of cement begin to expand with growing viscosity which will engender bonds among aggregates, sand, and clay. It should be mentioned that since clay minerals are chemically stable, they can scarcely

**Table 4** Mixture proportions of PIC-NZ

mix ID	natural zeolite (% of cement)	water ( $\text{kg}/\text{m}^3$ )	cement ( $\text{kg}/\text{m}^3$ )	Bentonite ( $\text{kg}/\text{m}^3$ )	gravel ( $\text{kg}/\text{m}^3$ )		sand ( $\text{kg}/\text{m}^3$ )
					4.75–9.5 (mm)	9.5–19 (mm)	
PIC-NZ0	0	450	152.7	30.5	475.8	279.4	617.9
PIC-NZ10	10	450	137.43	30.5	475.8	279.4	617.9
PIC-NZ15	15	450	129.79	30.5	475.8	279.4	617.9
PIC-NZ20	20	450	122.16	30.5	475.8	279.4	617.9
PIC-NZ25	25	450	114.54	30.5	475.8	279.4	617.9

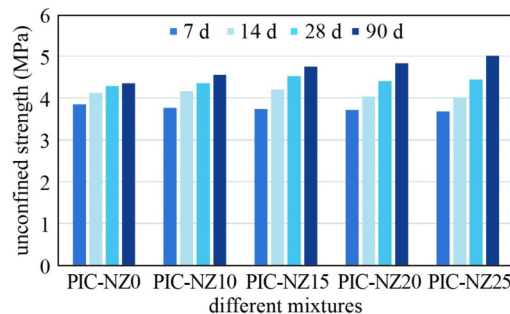


**Fig. 3** Evolution of compressive strength in different plastic concrete mixes.

participate in the hydration reactions [41]. In the presence of water, the surface of cement particles carry huge positive charge which attracts the negative charge on the surface of the clay particles. As a result of that, cement particles' surface absorb the clay particles. Because of the attractive forces between negative and positive charges, a considerable amount of water molecules will be absorbed by clay particles. In this regard, some of the free water molecules will be transformed into compound water molecules bound to clay, which will decrease the amount of free water that participates in cement hydration.

Moreover, as can be seen, at the early ages increasing the amount of natural zeolite replacement decreased the compressive strength of PIC-NZ specimens. The compressive strengths of PIC-NZ20 and PIC-NZ25 are 3.6% and 4.4%, respectively, lower than that of PIC-NZ0 at the age of 7 d. The rate of pozzolanic activity of zeolite is lower than that of the cement hydration at the early ages, which is related to the reduction in the compressive strength of PIC-NZ specimens containing higher proportions of NZ. At later ages, on the other hand, the compressive strength of specimens containing higher percentages of natural zeolite is much higher than that of the reference mixture. To be more specific, the compressive strengths of PIC-NZ20 and PIC-NZ25 are 11% and 15.1% higher, respectively, than that of the PIC-NZ0 at the age of 90 d. The compressive strength of materials containing zeolite is dependent on curing conditions, clinoptilolite particle size, and  $\text{Ca}(\text{OH})_2$  content [22]. By extending the curing time, the amount of portlandite will increase, which will increase the pozzolanic reactions. In this regard, the PIC-NZ specimens containing higher percentages of natural zeolite showed higher compressive strength.

Figure 4 illustrates the triaxial compression behavior of PIC-NZ specimens at the same confining pressure of 200 kPa. As can be seen, at the early ages, increasing the amount of natural zeolite replacement decreases the peak strength of specimens. This could be explained by the lower rate of pozzolanic activity of NZ relative to the rate of cement hydration, which consequently delivers the lower rates of strength development and heat liberation.

By extension of curing time, an enhancement of the specimens' strength happened due to the development of pozzolanic reactions. As illustrated in Fig. 4(b), specimens containing higher percentages of natural zeolite replacement show higher peak strength.

Furthermore, the passage of time affects the mode of failure. As can be seen in Fig. 4, the behavior of specimens at the age of 7 d is more likely to be ductile, but when curing time becomes longer, specimens show more brittle behavior (Fig. 4(b)). Consistently with this, the axial strain of specimens appertaining to peak strength ( $\varepsilon_a$ ) happened to a lesser extent at somewhat later ages compared to early ages, and then reaching a plateau as time progressed. An increase in the percentage of natural zeolite replacement at the age of 7 d caused more ductile behavior, and at the age of 90 d, it caused more brittle behavior.

### 3.1.2 Effect of confining pressure

Figure 5 depicts the effect of three different confining pressures of 200, 350, and 500 kPa on the triaxial compression behavior of PIC-NZ15. As illustrated in Fig. 5, although increasing the confining pressure up to

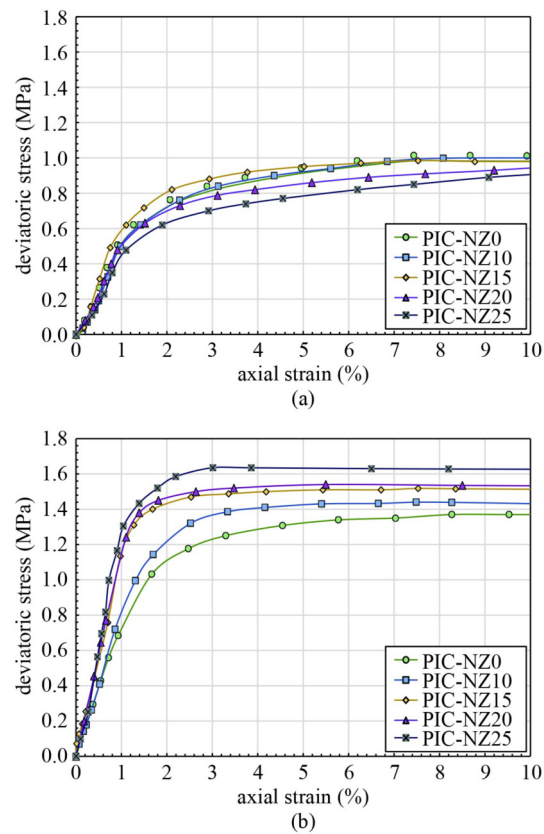


**Fig. 4** (a) Effect of zeolite content and specimen age on the triaxial compression behavior of PIC-NZ specimens in 7 d; (b) effect of zeolite content and specimen age on the triaxial compression behavior of PIC-NZ specimens in 90 d.

350 kPa increases the peak strength of the PIC-NZ15 specimens, an increase of confining pressure from 350 to 500 kPa decreased the peak strength. That is, increasing the confining pressure up to 500 kPa caused bond deterioration in PIC-NZ15 specimens. This can be seen at both ages 7 and 28 d. **Figure 6** illustrates this phenomenon at three different curing times.

**Figure 7** illustrates the effect of confining pressure on the PIC-NZ25 specimens to explore the bond deterioration in mixtures containing higher proportions of natural zeolite. As shown in **Fig. 7(a)**, the peak strength of specimens at the age of 7 d decreased by increasing the

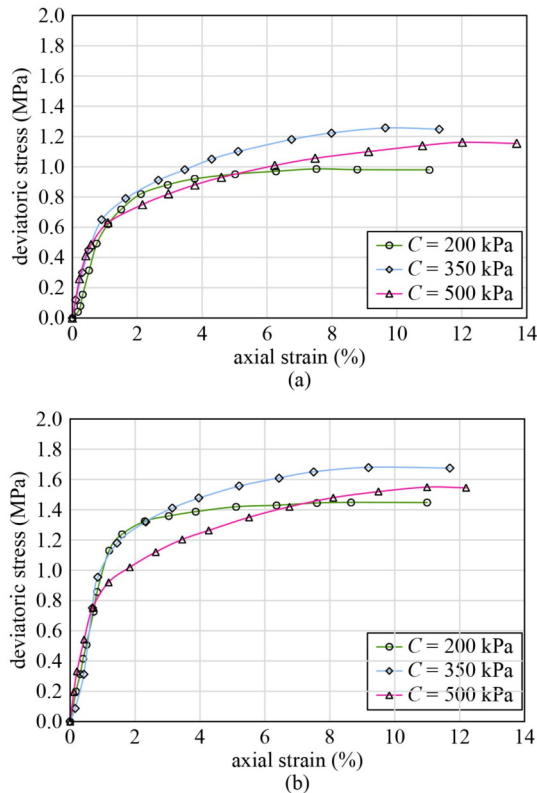


**Fig. 5** (a) Effect of confining pressure on the triaxial compression behavior of PIC-NZ15 specimens in 7 d; (b) effect of confining pressure on the triaxial compression behavior of PIC-NZ15 specimens in 28 d.

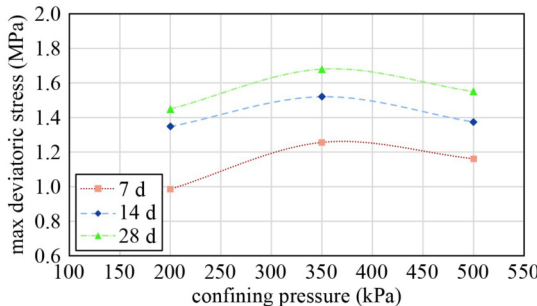


**Fig. 6** Effect of confining pressure on the peak strength of PIC-NZ15 specimens in different ages.

confining pressure from 200 to 350 kPa as well as when it increases from 350 to 500 kPa. The former case was not observed in the PIC-NZ15 specimens. At the early ages, the lower amount of cement hydration in PIC-NZ25 specimens and the slow rate of pozzolanic activities of natural zeolite led to the weaker bonds compared to those of PIC-NZ15. Furthermore, as shown in **Fig. 7(b)**, by extending the curing time and increasing the pozzolanic activities, increasing the confining pressure from 200 to 350 kPa did not produce a decrease in peak strength of PIC-NZ25 specimens. **Figure 8** shows the effect of confining pressure on the maximum deviatoric stress of PIC-NZ25 specimens at different curing ages.

The results show that increasing confining pressure caused specimens to adopt strain hardening behavior. By increasing the confining pressure, the axial strain of specimens that appertain to its peak strength ( $\varepsilon_a$ ) was increased. This phenomenon is illustrated in **Fig. 9** for PIC-NZ25.

**Figure 10** illustrates the effect of different confining pressures on crack patterns of PIC-NZ25 at the end of each test. Scale effects and specimen size are two factors that strongly influence the engineering properties of fractured media. As such, the results obtained from this

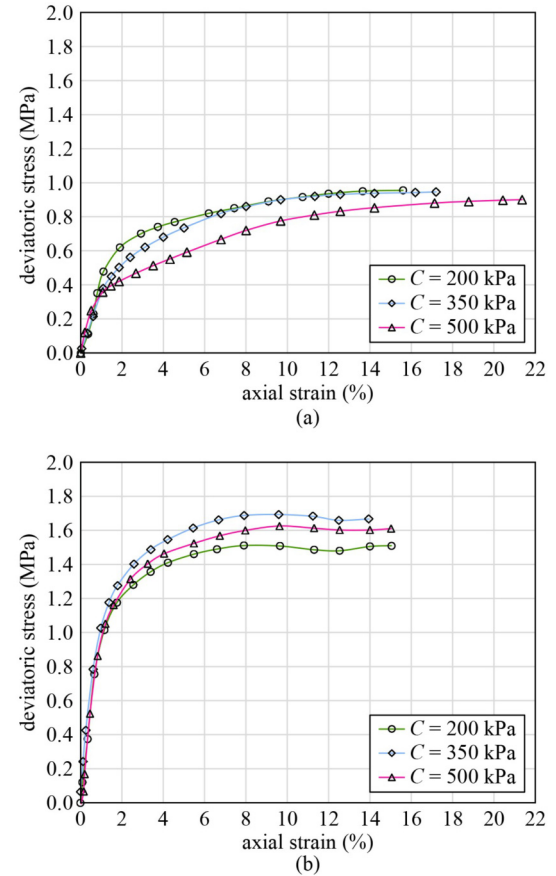


**Fig. 7** (a) Effect of confining pressure on the triaxial compression behavior of PIC-NZ25 specimens in 7 d; (b) effect of confining pressure on the triaxial compression behavior of PIC-NZ25 specimens in 28 d.

research should be considered as a primary behavior approximation of the *in-situ* PIC-NZ. Figure 10(a) shows the effect of consistent confining pressure of 350 kPa on PIC-NZ25 at the age of 28 d. As can be seen, the failure mode was made up of a well-defined failure plane. After that, increase in confining pressure to 500 kPa caused a change in the failure mode. As illustrated in Fig. 10(b), at the constant confining pressure of 500 kPa, a mixed failure mode was made up of a cracking parallel to specimen axes and a well-defined failure plane. These observations are similar to those obtained by Ref. [42].

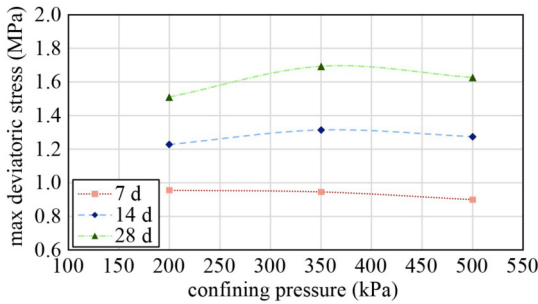


**Fig. 8** Effect of confining pressure on the peak strength of PIC-NZ25 specimens in different ages.

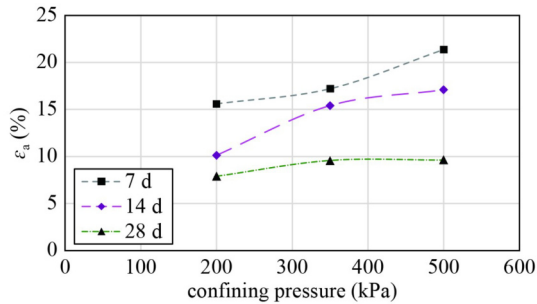


**Fig. 9** Effect of confining pressure on  $\epsilon_a$  of PIC-NZ25 at different ages.

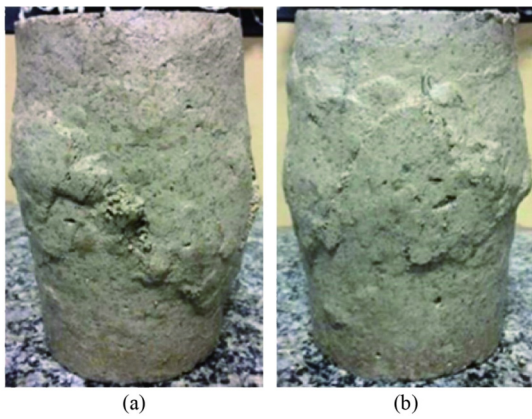


**Fig. 10** (a) Effect of confining pressure on the mode of failure of PIC-NZ25 at the age of 28 d at 350 kPa; (b) effect of confining pressure on the mode of failure of PIC-NZ25 at the age of 28 d at 500 kPa.

### 3.1.3 Effect of sulfate ions

Figures 11 and 12, respectively, illustrate the effect of sulfate ions on the unconfined strength and elastic modulus of PIC-NZ specimens. Being cured in the sulfate environment for 90 d increased the unconfined strength and modulus of elasticity of PIC specimens. As illustrated in Figs. 11 and 12, the ettringite that was produced decreased the porosity of the PIC-NZ specimens, which increased the unconfined strength and elastic modulus. In fact, in general when the ingress of sulfate ions happens, they firstly react with calcium ions from calcium silicate hydrate (C-S-H) or portlandite (CH) to form gypsum ( $\text{CaSO}_4 \cdot 2\text{H}_2\text{O}$ ). The decalcification of calcium silicate hydrate (C-S-H) and calcium hydroxide (CH) leads to the diffusion of calcium ions toward the outside medium. After that, the chemical reactions of hydrated calcium aluminates, such as monosulfate ( $\text{C}_4\text{AS}_1\text{H}_{12}$ ), tetracalcium aluminate ( $\text{C}_4\text{AH}_{13}$ ), and tricalcium aluminate ( $\text{C}_3\text{A}$ ) with secondary gypsum ( $\text{CaSO}_4 \cdot 2\text{H}_2\text{O}$ ) produce ettringite ( $\text{C}_6\text{AS}_3\text{H}_{32}$ ) [43,44]. Ettringite and gypsum are expansive materials; however, before they begin to exert pressure on pore walls, they will fill the capillary pores in empty spaces. There is a delay time (incubation period) before the macroscopic expansions begin and cause microcracks through the specimens. As can be seen in the figures, before the 90 d curing time, sulfate environment did not cause any drop in mechanical properties of PIC-NZ specimens. Moreover, the pozzolanic reaction of zeolite

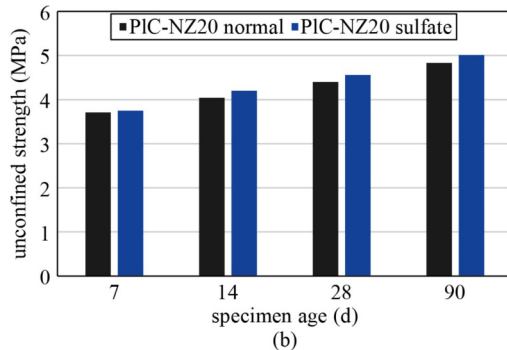
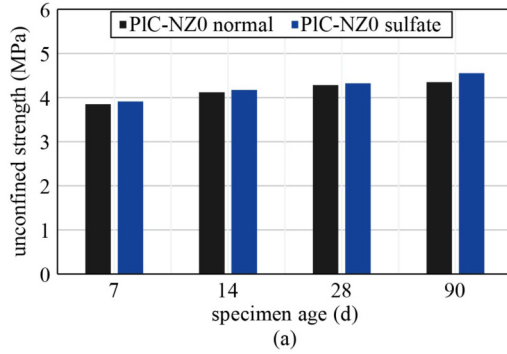


**Fig. 11** Effect of sulfate ions on the unconfined strength of (a) PIC-NZ0 and (b) PIC-NZ20 by the passage of time.

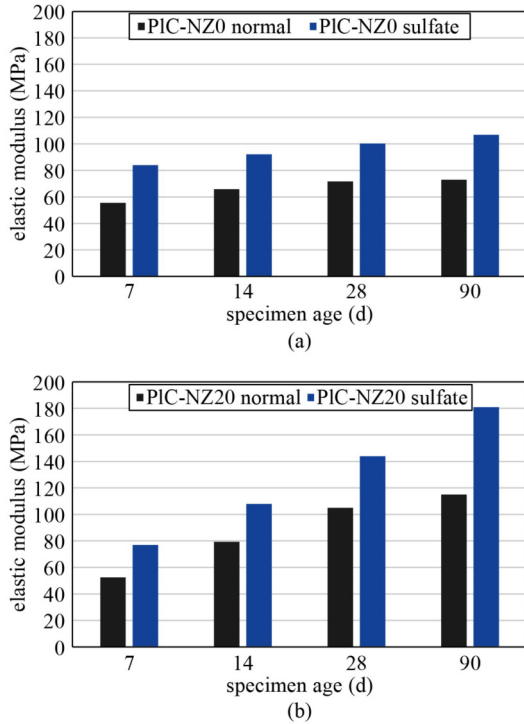


**Fig. 12** Effect of sulfate ions on the elastic modulus of (a) PIC-NZ0 and (b) PIC-NZ20 by the passage of time (at a constant confining pressure of 200 kPa).

with portlandite reduced the formation of gypsum in Portland cement-zeolite systems. A gradual chemical bonding of zeolite including large amounts of reactive  $\text{Al}_2\text{O}_3$  and  $\text{SiO}_2$  by  $\text{Ca}(\text{OH})_2$  caused the formation of dense gel-like hydration products of C-S-A-H and C-S-H type rather than gypsum. Substituting cement with zeolite led to a more profound reduction in the volume of the arising solids and more evident elimination of damaging expansion relative to those occurring when Portland cement alone was used and exposed to sulfate. However, as the reactive transport of sulfate ions progressed, ettringite and gypsum slowly filled all the pores in concrete. After the passage of the incubation period, as these products expanded more, they caused expansion stresses on pore walls. In fact, when the accumulation of ettringite in the interfacial transition zone became high it could easily cause expansion and further damage to concrete [44].

### 3.1.4 Elastic modulus

Figure 13 outlines the effect of specimen age and zeolite content on the elastic modulus of PIC-NZ specimens. The modulus of elasticity is a measure of interatomic bonding forces, which could be affected by the microstructural changes [45]. Chemical reactions mainly control the hydration process at the early stages. During this period, calcium silicate hydrate gel starts to spread on the surface of clinkers and creates a hydration shell that has low

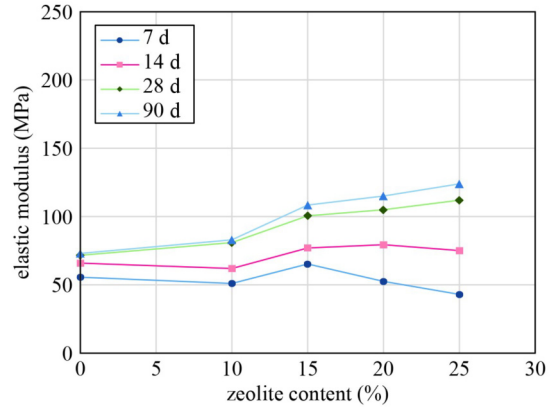


**Fig. 13** Effect of specimen age on the elastic modulus of PIC-NZ specimens.

rigidity. While the inner products of the hydration process keep developing with high Young's modulus and density, the outer products of hydration diffuse. As the hydration shell becomes thicker, ion diffusion starts to be the basic factor in controlling the chemical dynamic behavior in the hydration process. As a result of overlapping between crystals, the hydration products and dispersed clinkers bond together. Whilst the solid phases attach across the hydration space, the chaotic structure of the cement paste alters to a matrix inclusion structure that delivers a certain strength. The extension of curing time causes an increase in the modulus of elasticity of PIC-NZ specimens. Although being subjected to sulfate ions and utilizing natural zeolite has increased the elastic modulus of PIC-NZ specimens, this amount is still in the range that ICOLD recommends.

As illustrated in Fig. 13, at the age of 7 d, except for the elastic modulus of PIC-NZ15, increasing the zeolite content caused a decrease in the elastic modulus. For instance, the elastic moduli of PIC-NZ10 and PIC-NZ25 at the age of 7 d were recorded as 8.1% and 22.5% less than that of PIC-NZ0, respectively. This could be related to the slow rate of pozzolanic activities at the early ages during the cement hydration. It was supposed that a considerable amount of natural zeolite did not directly participate in the hydration process, which made it play the role of fine filler. By extension of curing time, on the other hand, the pozzolanic reactions led to an increase in the elastic modulus. As shown in Fig. 13, an increase in zeolite content increased the elastic modulus of specimens at the later ages. The elastic moduli of PIC-NZ10 and PIC-NZ25 at the age of 90 d were recorded as 13.6% and 69.8% higher, respectively, than the elastic modulus of PIC-NZ0 at the same age. By the passage of time, pozzolanic reaction products filled the capillary voids in the hydrated cement paste which decreased the porosity, and as a result the modulus of elasticity of specimens increased [45]. From 7–90 d of curing, a dramatic accretion in the elastic modulus is shown for mixtures with the replacement of NZ. For instance, the 90

d elastic modulus of PIC-NZ20 and PIC-NZ25 increased by 119% and 188% (compared to 7 d elastic modulus), respectively, whereas this increment was recorded 31.4% for PIC-NZ0.

**Figure 14** represents the effects of three different confining pressures on the elastic modulus of PIC-NZ15 specimens. It shows that an increase in confining pressure up to 350 kPa increased the elastic modulus. On the other hand, an increase in confining pressure from 200 to 500 kPa led to a decrease in elastic modulus at an early age and an increase of this amount at the later ages. Also, in all ages (up to 28 d), elastic modulus decreased with an increase in confining pressure from 350 to 500 kPa. As mentioned earlier, this could be related to the bond deterioration of specimens when they were subjected to high confining pressures. In fact, the strength development in blended cement is dependent on three main factors: the filler effect, the dilution effect, and the reactions between  $\text{Ca}(\text{OH})_2$  and pozzolanic materials [46]. The decrease in strength of bonds between 1 and 7 d was related and the filler effect and dilution effect [47,48]. On the other hand, with the passage of time, the pozzolanic reaction between natural zeolite and  $\text{Ca}(\text{OH})_2$  increased the strength of bonds in PIC-NZ specimens.

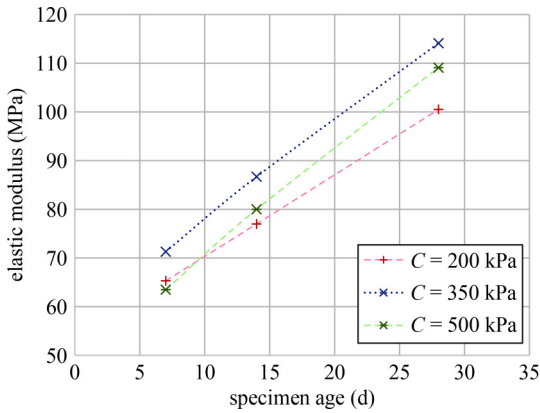


**Fig. 14** Effect of confining pressure on the elastic modulus of PIC-NZ15 specimens.

The decrease which happened by an increase in confining pressure from 350 to 500 kPa decreased with the passage of curing time.

**Figure 15** represents the effect of zeolite content on elastic modulus and peak strength of PIC-NZ specimens at the constant confining pressure of 200 kPa. The results show that an increase in zeolite content increased the gradient of lines. From this, it can be concluded that an increase in zeolite content had more influence on elastic modulus than on the peak strength of PIC-NZ specimens. In fact, the relationship between compressive strength and elastic modulus of concrete is dependent on the composition of concrete. Since the modulus of elasticity of concrete is a cardinal parameter in reinforced concrete design and analysis [49], the results obtained from this research could be considered as a primary behavior approximation of reinforced concrete design using natural zeolite.

### 3.2 Permeability of plastic concrete-natural zeolite

#### 3.2.1 Effect of zeolite content and specimen age

To explore the effect of zeolite content on the permeability, PIC-NZ specimens were tested when they were subjected to the confining pressure of 200 kPa. **Figure 16** shows the results. As illustrated in the figure, extending the curing time decreased the permeability of specimens. The continuity and the size of the pores in the microstructure of the PIC-NZ specimens determined its permeability. With the passage of time, as the pozzolanic reactions and hydration proceeded, the void space between particles gradually began to fill up with the products, which led to a decrease in permeability. Since the surface of bentonite has inordinate amounts of unsaturated chemical bonds ( $\text{Si}-\text{O}$  or  $\text{Al}-\text{O}$ ), hydration products use these chemical bonds as origin sites for their evolution [50]. Hydration products become oriented and grow along the direction of the pores, which has a huge refinement effect on the pores. Moreover, the porosity of

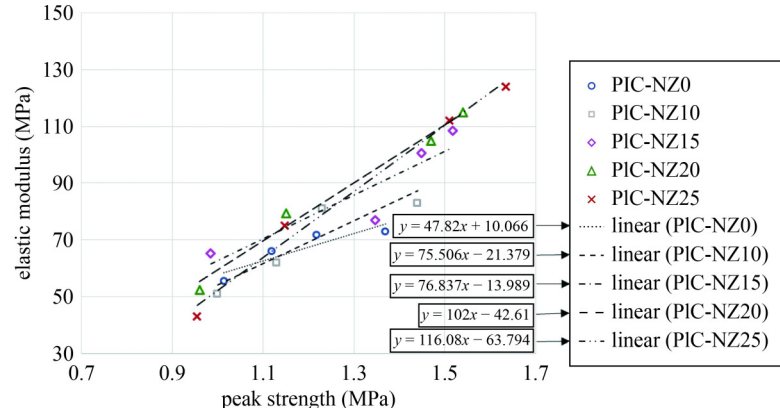


**Fig. 15** Effect of zeolite content and specimen age on the elastic modulus and peak strength of PIC-NZ specimens.

specimens is dramatically decreased by the overlapping that happens between adjacent products. On the other hand, bentonite fills the large pores that are present in the products of hydration, which will reduce the permeability of specimens by the passage of time. Furthermore, specimens containing higher proportions of natural zeolite showed lower amounts of permeability, which contributed to the products of the pozzolanic reactions.

### 3.2.2 Effect of confining pressure

To explore the effect of confining pressure on the coefficient of permeability of PIC-NZ specimens, three different confining pressures of 200, 350, and 500 kPa were used. Figure 17 represents the permeability of PIC-NZ10 at different confining pressures. It is clear that increasing the confining pressure reduces the size of the pores in specimens, which leads to lower coefficient of permeability [38]. In fact, most of the voids between cement and natural zeolite particles and their products are filled with bentonite, which reduces the permeability of PIC. Moreover, through the actions of negative and

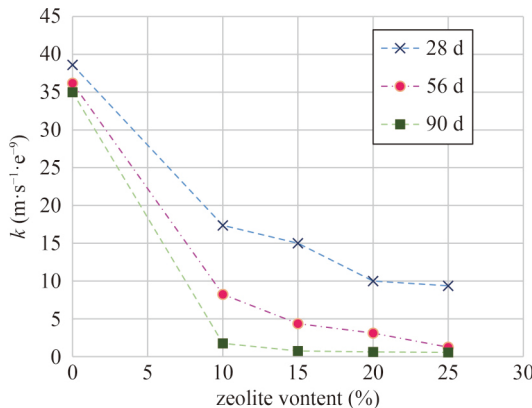


**Fig. 16** Effect of specimen age and zeolite content on the permeability of PIC-NZ specimen ( $C = 200$  kPa).

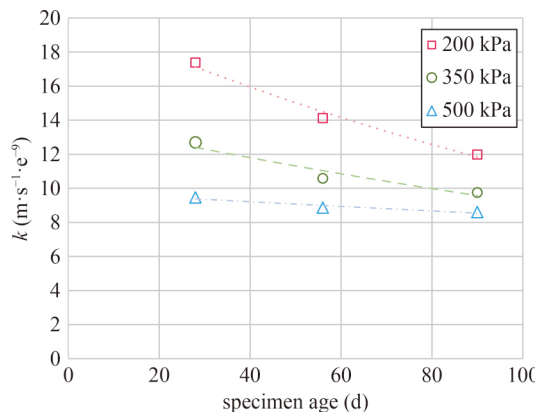


**Fig. 17** Effect of confining pressure on the permeability of PIC-NZ10.

positive charges, bentonite particles absorb a huge amount of free water molecules and turn most of them into combined water molecules, which depletes the area of water seepage. Therefore, the permeability of PIC-NZ specimens decreases [51]. Moreover, as can be seen in Fig. 17, at a high confining pressure of 500 kPa, the coefficient of permeability is not dependent on the age of the specimen.

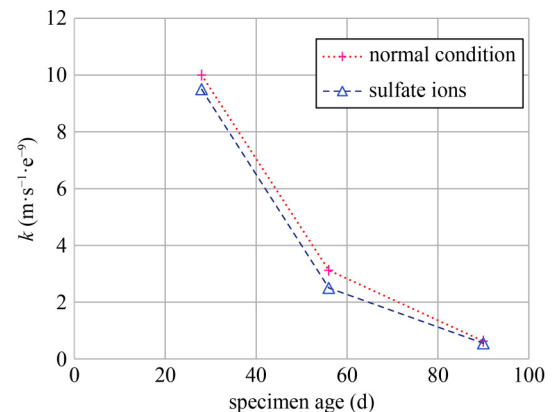
### 3.2.3 Effect of sulfate ions

Figure 18 illustrates the effects of the sulfate environment on the permeability of PIC-NZ20 specimens. Specimens that cured in the sulfate environment showed lower permeability. This is related to the progress of hydration action together with the filling and compaction action by the sulfate environment products during the incubation period. Ettringite crystals can fill cracks and voids, and they are usually 20 to 30 micrometers long and 2 to 4 micrometers in cross-section. On the other hand, it is anticipated that utilizing natural zeolite prolong the incubation period, since pozzolanic reaction leads to a compacted microstructure which decreases the amount of sulfate solution that can exist in the pore spaces of the specimens.

### 3.3 Scanning electron microscopy results

Figure 19 illustrates the effect of Pozzolanic reactions and cement hydration on the microstructure of PIC-NZ25 with the passage of time, using SEM images. Indeed, extending the curing time led to a decrease in the porosity of PIC-NZ specimens. Figure 19(a) manifests voids or capillary cavities which existed when the spaces were originally filled with water and did not fill with the hydration products of cement [45]. On the other hand, by extending the curing time, the size of the capillary voids will decrease, as illustrated in Fig. 19(b).

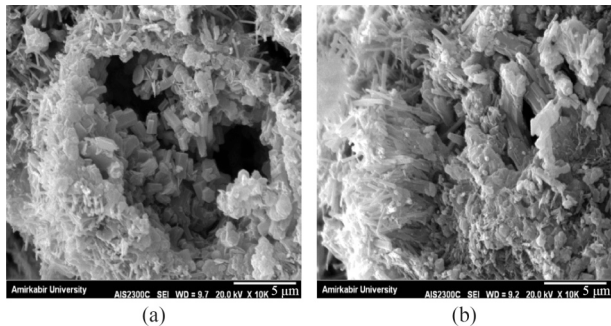
Extending the curing time will engender the



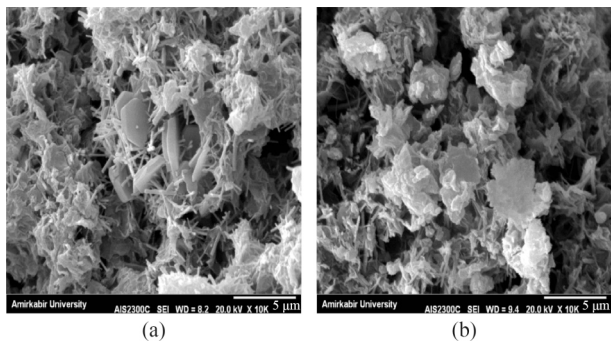
**Fig. 18** Effect of Sulfate ions on the permeability of PIC-NZ20 specimens by the passage of time ( $C = 200$  kPa).

consumption of  $\text{Ca}(\text{OH})_2$ . The distinctive hexagonal-prism morphology of large crystals of calcium hydroxide is illustrated in Fig. 20(a). The morphology of  $\text{Ca}(\text{OH})_2$  crystals rests on the temperature of hydration, space availability, and impurities present in the system [45]. The needle-shaped prismatic crystals of trisulfate hydrate can also be seen in Fig. 20(a).

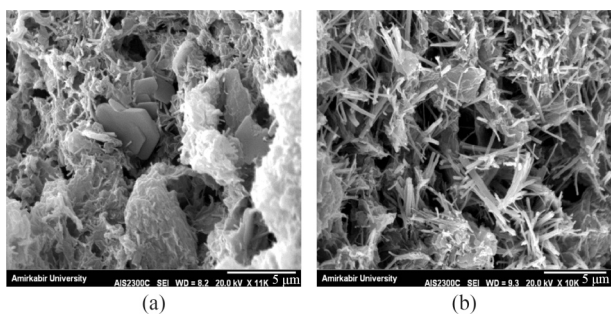
Figure 21 depicts the effect of sulfate ions on the evolution of ettringite in the PIC-NZ10 specimens. As illustrated in Fig. 21(b), specimens cured in the sulfate environment showed more conspicuous ettringite. The presence of ettringite decreased the porosity of specimens.



**Fig. 19** Effect of specimen age on porosity of PIC-NZ25 specimens: (a) 7 d and (b) 28 d.



**Fig. 20** Effect of specimen age on the consumption of  $\text{Ca}(\text{OH})_2$  in PIC-NZ15: (a) 7 d and (b) 28 d.



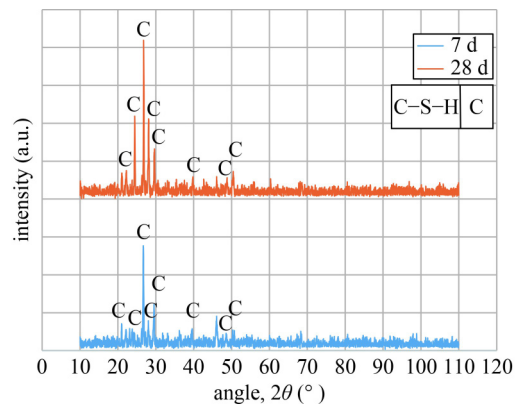
**Fig. 21** Evolution of ettringite in the PIC-NZ10 environment: (a) cured in a normal environment and (b) cured in sulfate environment.

Figure 22 illustrates the intensity vs. angle diffractogram of calcium silicate hydrate at different  $2\theta$  positions for PIC-NZ15. As shown in the XRD patterns, the peak values of C-S-H gel were higher at the age of 28 d than at the age of 7 d. Calcium silicate hydrate significantly affects the overall strength of concrete because it improves the bonding between cement and aggregates. The higher compressive strength of PIC-NZ15 at the age of 28 d compared to that at the age of 7 d was related to the higher peak values in the XRD analysis.

XRD diffraction patterns of PIC-NZ20 specimens that were cured in two different environments are illustrated in Fig. 23. As can be seen, specimens cured in the presence of sulfate ions showed higher peak values of ettringite. Ettringite formation reduced the porosity of concrete, which can help in increasing the durability of concrete.

#### 4 Conclusions

The uniaxial and triaxial behavior, the coefficient of



**Fig. 22** XRD diffraction patterns of PIC-NZ15 at two different ages.

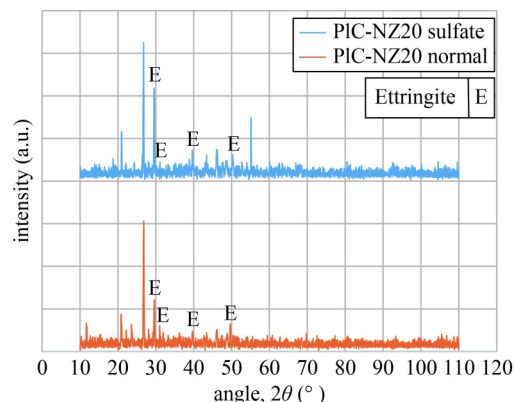


**Fig. 23** XRD diffraction pattern of PIC-NZ20 which have been cured in two different environments.

permeability in confined conditions, and microstructure of PIC-NZ specimens produced by partial replacement (10%–25%) of Portland cement with natural zeolite at different ages (7–90 d) were studied in this paper. The results showed that the replacement of cement by natural zeolite in PIC mix designs may not only improve the ability of cut-off walls for containment of heavy metals, but may also improve the mechanical properties of PIC specimens. Here are some significant conclusions.

1) Extending the curing time (7–90 d) led to the increase of cement hydration and pozzolanic activities which caused an increase in unconfined strength, peak strength, and elastic modulus of PIC-NZ specimens. For instance, from 7–90 d of curing, the elastic modulus of PIC-NZ0 and PIC-NZ20 increased 31.4% and 119%, respectively.

2) At the early ages (7 d) increase in the zeolite content led to a decrease in the unconfined strength of PIC-NZ specimens. For instance, at the age of 7 d, the compressive strength of PIC-NZ20 and PIC-NZ25 decreased by 3.6% and 4.4%, respectively, compared to the compressive strength of PIC-NZ0. However, for later ages, results showed that specimens that had a higher percentage of zeolite replacement achieved higher unconfined strength. To be more specific, the compressive strengths of PIC-NZ20 and PIC-NZ25 were 11% and 15.1% higher, respectively, than the compressive strength of PIC-NZ0 at the age of 90 d.

3) Considering the triaxial test results in different confining pressures, an increase in confining pressure from 200 up to 350 kPa led to an increase in peak strength and elastic modulus of PIC-NZ specimens. After that, increasing the confining pressure from 350 to 500 kPa caused a decrease in peak strength and elastic modulus of PIC-NZ specimens. This can be related to the bond deterioration of specimens in high confining pressure.

4) Increasing the confining pressure changed the mode of failure of PIC-NZ specimens in the triaxial compression test. At confining pressure of 350 kPa, the failure mode was made up of a well-defined failure plane. The failure mode of the PIC-NZ specimen in confining pressure of 500 kPa was a mixed failure mode, made up of a well-defined failure plane and a cracking parallel to specimen axes. Moreover, the increase in confining pressure increased the axial strain of the specimen that related to its peak stress.

5) Increase in zeolite content affected elastic modulus more than it affected the peak strength of PIC-NZ specimens.

6) Increasing the zeolite content decreased the coefficient of permeability of PIC-NZ specimens at later ages. Moreover, increasing the confining pressure led to a decrease in the coefficient of permeability.

7) Specimens cured in the presence of sulfate ions

manifested lower permeability and higher unconfined strength, elastic modulus, and peak strength due to reduced porosity.

## References

1. Alós Shepherd D, Kotan E, Dehn F. Plastic concrete for cut-off walls: A review. *Construction & Building Materials*, 2020, 255: 119248
2. Song S, You P. Performance of plastic concrete under true tri-axial compressive stress. *Construction & Building Materials*, 2021, 266: 121106
3. Ghanizadeh A R, Abbaslou H, Amlashi A T, Alidoust P. Modeling of bentonite/sepiolite plastic concrete compressive strength using artificial neural network and support vector machine. *Frontiers of Structural and Civil Engineering*, 2019, 13(1): 215–239
4. Amlashi A T, Abdollahi S M, Goodarzi S, Ghanizadeh A R. Soft computing based formulations for slump, compressive strength, and elastic modulus of bentonite plastic concrete. *Journal of Cleaner Production*, 2019, 230: 1197–1216
5. Juenger M C G, Siddique R. Recent advances in understanding the role of supplementary cementitious materials in concrete. *Cement and Concrete Research*, 2015, 78: 71–80
6. Wen L, Chai J, Xu Z, Qin Y, Li Y. Comparative and numerical analyses of response of concrete cutoff walls of earthen dams on alluvium foundations. *Journal of Geotechnical and Geoenvironmental Engineering*, 2019, 145(10): 04019069
7. ICOLD. *Filling Materials for Watertight Cut off Walls*. Paris: International Committee of Large Dams, 1985
8. Feng N Q, Li G Z, Zang X W. High-strength and flowing concrete with a zeolitic mineral admixture. *Cement, Concrete and Aggregates*, 1990, 12(2): 61–69
9. Soroush A, Soroush M. Parameters affecting the thickness of bentonite cake in cutoff wall construction: Case study and physical modeling. *Canadian Geotechnical Journal*, 2005, 42(2): 646–654
10. Bagheri A R, Alibabaie M, Babaie M. Reduction in the permeability of plastic concrete for cut-off walls through utilization of silica fume. *Construction & Building Materials*, 2008, 22(6): 1247–1252
11. Jalal M, Fathi M, Farzad M. Effects of fly ash and TiO<sub>2</sub> nanoparticles on rheological, mechanical, microstructural and thermal properties of high strength self compacting concrete. *Mechanics of Materials*, 2013, 61: 11–27
12. Damtoft J S, Lukasik J, Herfort D, Sorrentino D, Gartner E M. Sustainable development and climate change initiatives. *Cement and Concrete Research*, 2008, 38(2): 115–127
13. Metha P K, Monteiro P J M. *Concrete—Microstructure, Properties and Materials*. McGraw-Hill Professional, 2001, 23913
14. Celik K. Development and characterization of sustainable self-consolidating concrete containing high volume of limestone powder and natural or calcined pozzolanic materials. Dissertation for the Doctoral Degree. Berkeley: University of California, Berkeley, 2015
15. Ochoa L, Hendrickson C, Asce M, Matthews H S. Economic input-output life-cycle assessment of US residential buildings. *Journal of Infrastructure Systems*, 2002, 8(4): 132–138
16. Augustine C, Byrne A, Gimon E, Goerner T, Hoffman I, Kammen

- D M, Kantner J, Levin J, Lipman T, Mileva A, Muren R, Paul S, Sapatari S, Thorsteinsson H, Tominks C. Redefining what's possible for clean energy by 2020. Gigaton Throwdown, San Francisco, 2009
17. USGS MCS. Cement Statistics and Information. Washington, DC: US Geological Survey, 2012
18. Van Oss H. Minerals Yearbook: Slag-Iron and Steel. Washington, DC: US Geological Survey, 2011
19. Mehta P K. Sustainable cements and concrete for the climate change era—A review. In: 2nd International Conference on Sustainable Construction Materials and Technologies. Aneona: American Society of Civil Engineers, 2010
20. Ören A H, Kaya A, Kayalar A S. Hydraulic conductivity of zeolite-bentonite mixtures in comparison with sand-bentonite mixtures. *Canadian Geotechnical Journal*, 2011, 48(9): 1343–1353
21. Giosuè C, Mobili A, Yu Q L, Brouwers H J H, Ruello M L, Tittarelli F. Properties of multifunctional lightweight mortars containing zeolite and natural fibers. *Journal of Sustainable Cement-Based Materials*, 2019, 8(4): 214–227
22. Janotka I, Krajčí L. Sulphate resistance and passivation ability of the mortar made from pozzolan cement with zeolite. *Journal of Thermal Analysis and Calorimetry*, 2008, 94(1): 7–14
23. Şahmaran M. The effect of replacement rate and fineness of natural zeolite on the rheological properties of cement-based grouts. *Canadian Journal of Civil Engineering*, 2008, 35(8): 796–806
24. Vieira G L, Schiavon J Z, Borges P M, da Silva S R, de Oliveira Andrade J J. Influence of recycled aggregate replacement and fly ash content in performance of pervious concrete mixtures. *Journal of Cleaner Production*, 2020, 271: 122665
25. Öncü S, Bilsel H. Effect of zeolite utilization on volume change and strength properties of expansive soil as landfill barrier. *Canadian Geotechnical Journal*, 2017, 54(9): 1320–1330
26. Li F, Zhou C, Yang P, Wang B, Hu J, Wei J, Yu Q. Direct synthesis of carbon nanotubes on fly ash particles to produce carbon nanotubes/fly ash composites. *Frontiers of Structural and Civil Engineering*, 2019, 13(6): 1405–1414
27. Sun D, Shi H, Wu K, Miramini S, Li B, Zhang L. Influence of aggregate surface treatment on corrosion resistance of cement composite under chloride attack. *Construction & Building Materials*, 2020, 248: 118636
28. Neville A. The confused world of sulfate attack on concrete. *Cement and Concrete Research*, 2004, 34(8): 1275–1296
29. ACI Committee 201. Guide to Durable Concrete. American Concrete Institute, 2001
30. Haufe J, Vollpracht A. Tensile strength of concrete exposed to sulfate attack. *Cement and Concrete Research*, 2019, 116: 81–88
31. Chen J, Bharata R, Yin T, Wang Q, Wang H, Zhang T. Assessment of sulfate attack and freeze-thaw cycle damage of cement-based materials by a nonlinear acoustic technique. *Materials and Structures*, 2017, 50(2): 105
32. Rasheeduzzafar, Al-Amoudi O S B, Abduljauwad S N, Maslehuddin M. Magnesium-sodium sulfate attack in plain and blended cements. *Journal of Materials in Civil Engineering*, 1994, 6(2): 201–222
33. Barger G S, Bayles J, Blair B, Brown D, Chen H, Conway T, Hawkins P. Ettringite formation and the performance of concrete. Portland Cement Association, 2001: 1–16
34. ASTM. Standard Specification for Portland Cement, ASTM C150. West Conshohocken, PA: ASTM, 2012
35. ASTM. Standard Test Method for Measuring the Exchange Complex and Cation Exchange Capacity of Inorganic Fine-Grained Soils 1, ASTM D7503-18. West Conshohocken, PA: ASTM, 2020
36. ASTM. Standard Test Method for Unconsolidated-Undrained Triaxial Compression Test on Cohesive Soils, ASTM D2850-3a. West Conshohocken, PA: ASTM, 2013
37. ASTM. Standard Test Method for Unconfined Compressive Strength of Cohesive Soil, ASTM D2166. West Conshohocken, PA: ASTM, 2006
38. Mahboubi A, Ajorloo A. Experimental study of the mechanical behavior of plastic concrete in triaxial compression. *Cement and Concrete Research*, 2005, 35(2): 412–419
39. Xu S, Shan J, Zhang L, Zhou L, Gao G, Hu S, Wang P. Dynamic compression behaviors of concrete under true triaxial confinement: An experimental technique. *Mechanics of Materials*, 2020, 140: 103220
40. Piotrowska E, Malecot Y, Ke Y. Experimental investigation of the effect of coarse aggregate shape and composition on concrete triaxial behavior. *Mechanics of Materials*, 2014, 79: 45–57
41. Fu Z, Su H, Wen Z. Multi-scale numerical analysis for linear elastic behavior of clay concrete. *International Journal of Solids and Structures*, 2020, 203: 23–45
42. Hinchberger S, Weck J, Newson T. Mechanical and hydraulic characterization of plastic concrete for seepage cut-off walls. *Canadian Geotechnical Journal*, 2010, 47(4): 461–471
43. Sun D, Wu K, Shi H, Miramini S, Zhang L. Deformation behaviour of concrete materials under the sulfate attack. *Construction & Building Materials*, 2019, 210: 232–241
44. Sun D, Wu K, Shi H, Zhang L, Zhang L. Effect of interfacial transition zone on the transport of sulfate ions in concrete. *Construction & Building Materials*, 2018, 192: 28–37
45. Metha P K, Monteiro P J M. Concrete: Microstructure, Properties, and Materials. 2nd ed. Hoboken, NJ: Prentice Hall, 1993
46. Badogiannis E, Kakali G, Dimopoulou G, Chaniotakis E, Tsivilis S. Metakaolin as a main cement constituent. Exploitation of poor Greek kaolins. *Cement and Concrete Composites*, 2005, 27(2): 197–203
47. Perraki T, Kontori E, Tsivilis S, Kakali G. The effect of zeolite on the properties and hydration of blended cements. *Cement and Concrete Composites*, 2010, 32(2): 128–133
48. Perraki T, Kakali G, Kontori E. Characterization and pozzolanic activity of thermally treated zeolite. *Journal of Thermal Analysis and Calorimetry*, 2005, 82(1): 109–113
49. Demir F, Armagan Korkmaz K. Prediction of lower and upper bounds of elastic modulus of high strength concrete. *Construction & Building Materials*, 2008, 22(7): 1385–1393
50. Liu X, Feng P, Li W, Geng G, Huang J, Gao Y, Mu S, Hong J. Effects of pH on the nano/micro structure of calcium silicate hydrate (C-S-H) under sulfate attack. *Cement and Concrete Research*, 2021, 140: 106306
51. Wang S, Wen Y, Fei K. Effects of pH and EC on the strength and permeability of plastic concrete cutoff walls. *Environmental Science and Pollution Research International*, 2021, 28(31): 42798–42806